An Enhanced SPEI Drought Monitoring Method Integrating Land Surface Characteristics

Liqing Peng[1*], Justin Sheffield[2], Zhongwang Wei[3], Michael Ek[4], Eric F. Wood[5†]

5   [1] Food Program, World Resources Institute, Washington DC, United States.
[2] School of Geography and Environmental Science, University of Southampton, Southampton, United Kingdom.
[3] Southern Marine Science and Engineering Guangdong Laboratory (Zhuhai), Guangdong Province Key Laboratory for Climate Change and Natural Disaster Studies, School of Atmospheric Sciences, Sun Yat-Sen University, Guangzhou, China.
10   [4] Joint Numerical Testbed, Research Applications Laboratory, National Center for Atmospheric Research, Boulder, Colorado, United States.
[5] Department of Civil and Environmental Engineering, Princeton University, Princeton, New Jersey, United States. (†Deceased)

15   *Correspondence to*: Liqing Peng (pengliqing51@gmail.com)

Abstract. Atmospheric evaporative demand is a key metric for monitoring agricultural drought. The existing ways of estimating evaporative demand in drought indices do not faithfully represent the constraints of land 20   surface characteristics and become less accurate over non-uniform land surfaces. This study proposes incorporating surface vegetation characteristics, such as vegetation dynamics data, aerodynamic and physiological parameters, into existing potential evapotranspiration (PET) methods. This approach is implemented over the Continental United States (CONUS) for the period of 1981-2017 and is tested in a recently developed drought index the Standardized Precipitation Evapotranspiration Index (SPEI). We show 25   that activating realistic maximum surface and aerodynamic conductance could improve prediction of soil moisture dynamics and drought impacts by 29% on average compared to the widely used simple methods, especially effective in the forests and humid regions. Surface characteristics that have a strong influence on the performance of the SPEI are mainly driven by leaf area index (LAI). Our approach only requires the minimum amount of ancillary data, while permitting both historical reconstruction and real-time forecast of 30   drought. This offers a physically meaningful, yet easy-to-implement way to account for the vegetation control in drought indices.

1 Introduction

35   Drought is one of the most costly hydrological hazards (Wilhite, 2000; Ross & Lott, 2003), with devastating impacts on croplands and pastures (Kogan, 1995), forests ecosystems (Clark et al., 2016), electricity production, water quality, and soil fertility (Loon, 2015). Monitoring the changes in water availability is critical for providing early warnings of drought and for risk management (Wilhite, Sivakumar, & Pulwarty, 2014). Many physical or probabilistic measures have been developed (Heim, 2002) to quantify drought, such

40   as Palmer Drought Severity Index (PDSI, Palmer, 1965), Standardized Precipitation Index (SPI, McKee, Doesken, Kleist, & others, 1993), Vegetation Condition Index (VCI, Kogan, 1995), and multiple remote sensing drought indices (Zhang, Jiao, Zhang, Huang, & Tong, 2017).

Atmospheric evaporative demand (AED) is a key input to drought indices because it is a measure of water demand, namely, how thirsty the atmosphere is (Peng, Li, & Sheffield, 2018). AED typically reflects the

45   effect of temperature and humidity, and is considered a major driver of drought stress on vegetation and tree mortality (Williams et al., 2012; McDowell et al., 2018). Among the drought indices, the recently developed Standardized Precipitation Evapotranspiration Index (SPEI) (Vicente-Serrano, Beguería, & López-Moreno, 2010) factors in water demand (AED) in addition to water supply (precipitation). Compared to the SPI that only considers precipitation, the SPEI is more suitable for quantifying the drought impacts on agriculture

50   (Potop, 2011; Potop, Možný, & Soukup, 2012), and ecosystems (Vicente-Serrano et al., 2012; Vicente-Serrano et al., 2013; Barbeta, Ogaya, & Peñuelas, 2013). In addition, the SPEI is more flexible than the PDSI because it is not sensitive to soil water field capacity and can be implemented on various time scales (Vicente-Serrano, der Schrier, Beguería, Azorin-Molina, & Lopez-Moreno, 2015; Zhao et al., 2017). It has been widely used for both drought reconstruction and monitoring (Paulo, Rosa, & Pereira, 2012; Beguería, Vicente-

55   Serrano, Reig, & Latorre, 2013).

The way of estimating AED in drought indices has a significant impact on drought quantification (Sheffield, Wood, & Roderick, 2012; Trenberth et al., 2013; Yang, Roderick, Zhang, McVicar, & Donohue, 2018; Dewes et al., 2017). AED is approximated by potential evapotranspiration (PET), the maximum rate of evapotranspiration when surface water supply is unlimited. Previous work has used various PET formulations

60   for AED in the SPEI since it was first proposed in 2010 (Vicente-Serrano, Beguería, & López-Moreno, 2010; Beguería, Vicente-Serrano, Reig, & Latorre, 2013). These conventional PET methods do not factor in the effects of surface characteristics. The vegetation control on transpiration is often neglected, and therefore the maximum surface conductance is overestimated and the PET rate during the onset and retreat of the growing season is unrealistically high. Furthermore, by assuming an smooth reference surface, some methods do not

65   account for surface roughness, hence downplay aerodynamic conductance and suppress the PET estimate

(Peng et al., 2019). Even though the reference evapotranspiration (ET_0) method (Allen, Pereira, Raes, & Smith, 1998) considers the biophysical limitation of transpiration by assigning a surface resistance under well-watered condition, it does not account for vegetation phenology (Lorenz, Davin, Lawrence, Stöckli, & Seneviratne, 2013) and assumes a fixed reference height and a constant surface resistance for all vegetation

70   types. This approach is not physically meaningful for forests, where canopy height is relatively large and vegetation cover varies significantly.

We hypothesize that adding the surface vegetation characteristics to an existing drought quantification approach will improve the spatial and temporal accuracy of drought prediction. The goals of this study are to explore which surface features are the most useful for enhancing drought prediction, and which vegetation

75   types benefit most from incorporating these features. We propose incorporating realistic vegetation restrictions into existing PET methods, while not increasing much cost and uncertainty caused by additional data sources and complex formulations. Then we use independent soil moisture observations (Dai, Trenberth, & Qian, 2004) from satellite to evaluate the drought depictions by various forms of PET approaches across different temporal scales. The evaluation against observed soil moisture allows the direct diagnosis of the

80   most sensitive surface characteristics and the most effective approach for drought quantification (Vicente-Serrano et al., 2012).

In this study, we focus on the continental U.S. (CONUS) primarily because the drought events hitting this region have raised interest in variability, trends, and future risks of drought (Andreadis & Lettenmaier, 2006; Hobbins et al., 2012; Dewes et al., 2017). Several most severe droughts hit the western U.S. in the recent

85   decade, including the 2012 Great Plains drought (Hoerling et al., 2014) and the 2012-2016 California drought (Dong et al., 2019). The western U.S. has been experiencing the most severe drought period after the 1930s and 1950s (Andreadis, Clark, Wood, Hamlet, & Lettenmaier, 2005), and its vulnerability to drought continued to grow (Andreadis & Lettenmaier, 2006). Besides, high-quality meteorological datasets are available over the CONUS (Daly et al., 2008; Xia et al., 2012) and can help reduce the uncertainty of drought

90   prediction originating from input forcings.

2 Data

2.1 Meteorology

To calculate the SPEI, we use high-quality meteorology data from PRISM (Parameter-elevation Regressions
on Independent Slopes Model) that employs weather stations and digital elevation model (Daly, Neilson, &
Phillips, 1994; Daly et al., 2008). We acquire daily precipitation, daily mean, maximum, minimum, and dew
point temperature on a 4 km grid for the period of 1981-2017. Surface downward shortwave and net longwave
radiation, pressure, and wind speed are taken from the NLDAS-2 (North American Land Data Assimilation
System phase 2 (Xia et al., 2012). All data are spatially restricted to the continental United States (25–50ºN,
67–125ºW) and regridded to the 0.125º NLDAS-2 grid using the first-order conservative remapping tool
provided by Climate Data Operators (https://code.zmaw.de/projects/cdo).

2.2 Soil moisture

The European Space Agency Climate Change Initiative (ESA CCI) v4.3 surface soil moisture (SMsurf) is
used to evaluate the drought severity quantified by the SPEI time series (https://www.esa-soilmoisture-
cci.org/). This dataset combines several active and passive microwave soil moisture products into a
harmonized surface layer soil moisture (2-5 cm) in m^3 m^{-3} (Liu et al., 2012; Gruber et al., 2017; Gruber et
al., 2019). The version 4.3 provides soil moisture on a 0.25º grid at daily time step for the 1979-2017 period
and has been widely used in ET and drought studies (Dorigo et al., 2017; Martens et al., 2017).

2.3 Land surface ancillary data

The land surface data used for deriving biophysical parameters include gridded land cover type, leaf area
index, and surface albedo. The land cover type is provided by the 0.5 km MODIS-based Global Land Cover
Climatology during the 2001-2010 period (Broxton, Zeng, Sulla-Menashe, & Troch, 2014,
https://archive.usgs.gov/archive/sites/landcover.usgs.gov/global_climatology.html). This dataset has 17 land
cover classes based on the International Geosphere‐Biosphere Program (IGBP) classification. This land
cover climatology dataset is displayed in Fig. 1.

The monthly climatology of leaf area index is obtained from the 15-day, 1 km AVHRR GIMMS LAI3g
product that covers the period of 1982-2016 (Zhu et al., 2013). The monthly climatology of surface albedo
is derived from the 8-day, 0.05º GLASS (Global Land Surface Satellite) albedo product. This
GLASS02A05/06 product combines MODIS and AVHRR (Advanced Very-High-Resolution Radiometer)
to provide a gap-filled land surface shortwave black-sky and white-sky albedo (Qu et al., 2014; Liu et al.,

2013) that covers the period of 1982-2012. The canopy height data are obtained from a global tree height dataset at 1-km for 2005 using spaceborne lidar (Simard et al., 2011).
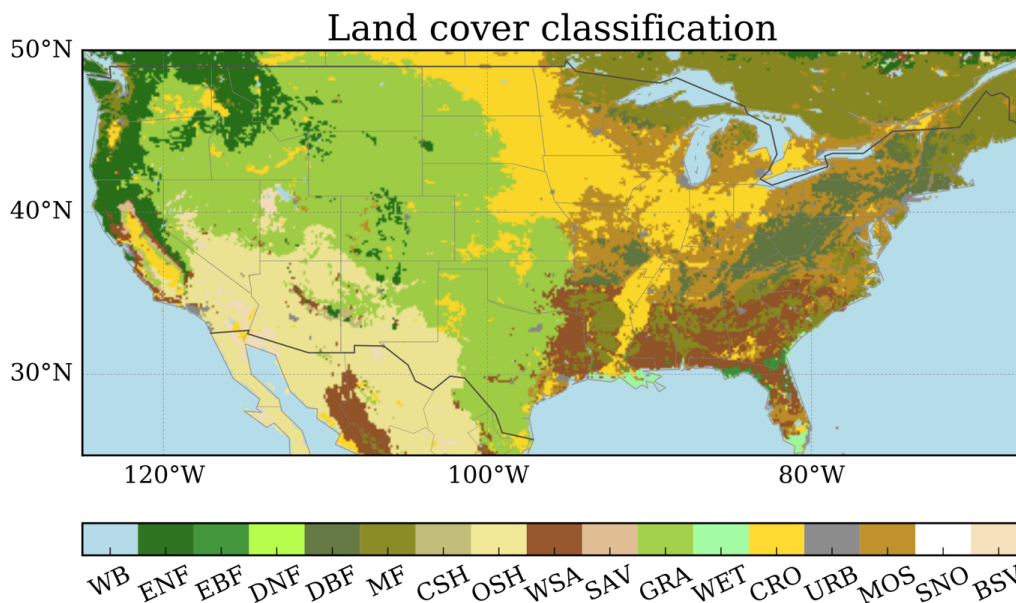
Figure 1. The land cover classification over the Continental United States used for surface vegetation
parameter inference. The classification is based on the satellite retrieval of land cover climatology
during 2001-2010 (see Table 1 for a list of land cover full names).

3 PET methods

3.1 Current PET methods

The Penman equation (Penman, 1948) is the most comprehensive physically-based method to estimate PET by combining the radiative and aerodynamic components:

$$PET_{Penman} = \frac{\Delta(R_n - G) + \rho_a C_p D Ga}{\lambda(\Delta + \gamma)} \tag{1}$$

where PET is expressed as water mass fluxes (kg m^{-2} s^{-1}), R_n is the surface net radiation (W m^{-2}), G is the surface ground heat flux (W m^{-2}), Δ is the slope of the saturation vapor pressure curve at the temperature of interest (Pa K^{-1}), γ is the psychrometric constant (Pa K^{-1}), λ is the latent heat of vaporization (J kg^{-1}), ρ_a is the air density (kg m^{-3}), C_p is the specific heat of air (J kg^{-1} K^{-1}), D is the vapor pressure deficit (VPD, Pa), and Ga is the aerodynamic conductance (m s^{-1}).

The variants of the Penman equation have been widely used to estimate PET in hydrological and land surface modeling (Sellers et al., 1996; Liang et al., 1994; Ek et al., 2003; Peng, Li, & Sheffield, 2018; Peng et al., 2019; Yang et al., 2019). The open-water Penman (OW) equation is a simplified Penman equation to calculate

140   PET over an open water surface, re-parameterized by Shuttleworth (1993):

$$PET_{OW} = \frac{\Delta}{(\Delta + \gamma)} \frac{(R_n - G)}{\lambda} + \frac{\gamma}{\Delta + \gamma} \frac{6.43(1 + 0.536u_2)D}{\lambda} \tag{2}$$

where PET_{OW} is typically in mm d^{-1} (kg m^{-2} s^{-1} = 86400 mm d^{-1}), $(R_n - G)$ is daily available energy (J m^{-2} d^{-1}), u_2 is the wind speed at 2-m height (m s^{-1}), λ is J kg^{-1}, and D is in kPa. Note that some of the variables have different units from Equation 1.

The Penman-Monteith (PM) equation (Monteith, 1965) is an extended version of the Penman equation to

145   estimate actual ET (kg m^{-2} s^{-1}), which introduces the surface conductance (Gs, m s^{-1}):

$$PET_{PM} = \frac{\Delta(R_n - G) + \rho_a C_p D Ga}{\lambda(\Delta + \gamma \left(1 + \frac{Ga}{Gs}\right))} \tag{3}$$

The reference crop evapotranspiration (PET_{RC}) recommended by the UN Food and Agricultural Organization (FAO) is a specific application of the Penman-Monteith equation (Allen, Pereira, Raes, & Smith, 1998). It is designed for calculating the maximum ET of reference crop under well-watered condition. The general formula is given by Allen et al. (2005):

$$PET_{RC} = \frac{0.408\Delta(R_n - G) + \frac{C_n u_2}{T_a + 273}\gamma D}{\Delta + \gamma(1 + C_d u_2)} \tag{4}$$

150   where PET_{RC} is also in mm d^{-1}, $(R_n - G)$ is daily available energy (MJ m^{-2} d^{-1}), Δ and γ are in kPa °C^{-1}, T_a is the air temperature at 2-m height (°C), D is in kPa, C_n (K mm s^3 Mg^{-1} d^{-1}) is a constant describing the effect of aerodynamic conductance (Ga) that increases with canopy height. The denominator $\Delta + \gamma(1 + C_d u_2)$ is a special form of the denominator of the Penman-Monteith equation $\Delta + \gamma(1 + Rs/Ra)$. C_d ($\frac{Rs}{Ra\,u_2}$, s m^{-1}) is a constant that increases with the ratio of surface resistance ($Rs = 1/Gs$) to aerodynamic resistance ($Ra = 1/Ga$). There are two sets of C_n and C_d, tall crop (C_n=1600, C_d=0.38) and short crop (C_n=900, C_d=0.34).

155   The FAO short crop equation is used in the recent version of the SPEI calculation (Beguería, Vicente-Serrano, Reig, & Latorre, 2013).

The Priestley-Taylor (PT) equation is also a simplified form of the Penman equation, which describes evaporation from a well-watered surface based on the equilibrium evaporation under conditions of minimal advection (Priestley & Taylor, 1972):

$$PET_{PT} = 1.26 \frac{\Delta(R_n - G)}{\lambda(\Delta + \gamma)} \tag{5}$$

where PET_{PT} is in mm d^{-1} and $(R_n - G)$ is in J m^{-2} d^{-1}. The above methods require observations or estimates of surface net radiation, near-surface temperature, wind speed, or specific humidity. Empirically based methods can induce large uncertainty in the drought projection (Sheffield et al., 2012; Feng, Trnka, Hayes, & Zhang, 2017) and are therefore not considered in the study.

3.2 Surface characteristics

Classical PET definitions rely on surface meteorology and do not faithfully represent the vegetation conditions and biophysical constraints and become less accurate over non-uniform land surfaces (Moran et al., 1996). To understand the impact of surface characteristics on the AED estimate and drought quantification, three factors are explored: (i) aerodynamic conductance, (ii) surface conductance, and (iii) surface albedo. This section introduces the major equations and formulas for these factors.

3.2.1 Aerodynamic conductance

Aerodynamic conductance Ga in the OW and PT methods (Equations 2 and 5) are implicitly derived from a smooth surface with low roughness length, which can underestimate the Ga and PET values in the forests (Peng et al., 2019). Open water aerodynamic conductance Ga_{ow} can be obtained by inverting the open water Penman equation (Equation 2) to match the Penman equation (Equation 1), given by Peng et al. (2019):

$$Ga_{ow} = \frac{6.43(1 + 0.536u_2) \cdot P_s}{86.4\epsilon\lambda\rho_a} \tag{6}$$

where u_2 is converted from wind speed at 10-m to 2-m height following the wind profile relationship in Allen, Pereira, Raes, & Smith (1998). P_s is near-surface atmospheric pressure (Pa), ϵ is the ratio of molecular weight of water to dry air (= 0.622).

Short reference crop aerodynamic conductance $Ga_{RC-short}$ and $Ga_{RC-tall}$ is given by

$$Ga_{RC-short} = \frac{u_2}{208} \tag{7}$$

$$Ga_{RC-tall} = \frac{u_2}{110} \tag{8}$$

180   where u_2 is converted from wind speed at 10-m to 2-m height (m s^{-1}).

Instead of the low Ga in OW and the fixed Ga in RC, it is better to use canopy height to generate more realistic surface roughness (Brutsaert & Stricker, 1979; Allen, Pereira, Raes, & Smith, 1998; Shuttleworth, 1993):

$$Ga = \frac{k^2 u_z}{\ln\left(\frac{z_m - d_0}{z_{0m}}\right)\ln\left(\frac{z_h - d_0}{z_{0h}}\right)} \tag{9}$$

where z_m is the measurement height (m) for wind speed, z_h is the measurement height (m) for temperature
185   and humidity, u_z is the wind speed at measurement height (m s^{-1}), k is the von Karman constant, d_0 is the zero-plane displacement height (m), z_{0m} and z_{0h} are the roughness lengths for momentum and heat (m). d_0 and z_{0m} can be estimated from canopy height (h) following d_0 = 2h/3 and z_{0m} = h/8 (Brutsaert, 1982). When estimating z_{0h}, instead of assuming $z_{0h} = 0.1z_{0m}$ as in Allen, Pereira, Raes, & Smith (1998), it is common to introduce a concept of excess resistance (Verma, 1989) and characterize the relationship between z_{0h} and
190   z_{0m}:

$$z_{0h} = \frac{z_{0m}}{\exp(kB^{-1})} \tag{10}$$

The $\ln(z_{0m}/z_{0h})$ term, also known as kB^{-1}, depends on the roughness Reynold's number $Re*$ or frictional velocity ($u*$), LAI (Yang & Friedl, 2003), and land cover type (Rigden, Li, & Salvucci, 2018).

Given that NLDAS-2 provides wind speed at a 10 m level, we used a measurement height = 10 m for both wind speed and temperature because the variation in the vertical temperature profile (2-10 m) is negligible
195   compared to that of wind speed. As canopy height and frictional velocity are rarely measured continuously for each grid, we use a simple look-up table approach to provide roughness parameters, z_{0m}, d_0, kB^{-1}, based on land cover type (Fig. 1), summarized in Table 1. z_{0h} is then estimated based on land cover specific z_{0m} and kB^{-1} (Equation 10). For z_{0m}, we apply the typical values for different land cover types, and estimated d_0 from z_{0m} ($d_0 \approx 16z_{0m}/3$).

200   For kB^{-1}, we adopt estimates from a collection of literature as below. The forests generally have lower kB^{-1} values (kB^{-1} = 1 for needleleaf or mixed forest, kB^{-1} = 0.5 for broadleaf) than shrublands (kB^{-1} = 3.75) and croplands (kB^{-1} = 1.75), based on the values of Rigden et al. (2018) for the medium emissivity case (ϵ = 0.96). For grasslands, kB^{-1} = 2.25 is computed as the average of short grass (kB^{-1} = 2.0) and medium-length grass (kB^{-1} = 2.5), based on Brutsaert (1982). For barren or bare soil, we estimate kB^{-1} = 3 by taking
205   the average of all observed kB^{-1} in Yang et al. (2008). Nadeau et al. (2009) suggested kB^{-1} = 6 for the

urban area. For water body, wetlands, and snow, we adopt the widely-used $kB^{-1} = 2$, as Zilitinkevich et al. (2001) showed that kB^{-1} over the water surface is within the 0~4 range. There are large variations in the observed kB^{-1} for savannas. Troufleau et al. (1997) reported $kB^{-1} = 7.9$ for fallow savanna; Kustas et al. (1989) provided a range of 1 to 11; Stewart et al. (1994) found an average value of $kB^{-1} = 5.8$, similar to the

210 study by Lhomme et al. (1997) that reported $kB^{-1} = 5.9$ for Sahelian vegetation; Verhoef et al. (1997) suggested a high value of $kB^{-1} = 12.4$. We choose $kB^{-1} = 7$ as most of these observed values fall into the range of 6-8.

Table 1. Ga and Gs parameters by IGBP land cover*.

ID	Code	Name	z_{0m} (m)	d_0 (m)	kB^{-1}	Gst_{max} [j] (mm s^{-1})	Rst_{min} [k] (s m^{-1})
0	WB	Water body	0.0004 [a]	0.002	2.0 [e]	NA	NA
1	ENF	Evergreen needleleaf	1.1 [b]	5.9	1.0 [f]	9.3	150
2	EBF	Evergreen broadleaf	1.1 [b]	5.9	0.5 [f]	9.3	150
3	DNF	Deciduous needleleaf	0.9 [b]	4.8	1.0 [f]	9.3	150
4	DBF	Deciduous broadleaf	0.9 [b]	4.8	0.5 [f]	9.3	150
5	MF	Mixed forest	0.9 [b]	4.8	1.0 [f]	9.3	150
6	CSH	Closed shrublands	0.2 [a]	1.1	3.75 [f]	9.3	150
7	OSH	Open shrublands	0.2 [a]	1.1	3.75 [f]	9.3	100
8	WSA	Woody savannas	0.4 [a]	2.1	7.0 [g]	9.3	180
9	SAV	Savannas	0.4 [a]	2.1	7.0 [g]	9.3	120
10	GRA	Grasslands	0.05 [a]	0.27	2.25 [a]	12	115
11	WET	Permanent wetlands	0.04 [c]	0.21	2.0 [e]	12	65
12	CRO	Croplands	0.12 [d]	0.64	1.75 [f]	12.2	90
13	URB	Urban and built up	1.1 [b]	5.9	6.0 [h]	NA	NA
14	MOS	Cropland/vegetation	0.12 [d]	0.64	1.75 [f]	12.2	120
15	SNO	Snow/ice	0.00001 [a]	5.3E-05	2.0 [e]	NA	NA
16	BSV	Barren	0.01 [d]	0.053	3.0 [i]	NA	NA

*The above estimates are collected from [a]Brutsaert (1982), [b]Campbell and Norman (1998), [c]Acreman et al.
215 (2003), [d]Monteith and Unsworth (2013), [e]Zilitinkevich et al. (2001), [f]Rigden et al. (2018), [g]Kustas et al. (1989), Stewart et al. (1994), Troufleau et al. (1997), Lhomme et al. (1997), and Verhoef et al. (1997), [h]Nadeau et al. (2009), [i]Yang et al. (2008), [j]Kelliher et al. (1995), [k]Zhou et al. (2006).

3.2.2 Surface conductance

220 The maximum surface conductance Gs_{max} can be obtained by scaling the maximum stomatal conductance (Gst_{max}) with the LAI satellite data (Yan et al., 2012):

$$Gs_{max} = Gst_{max} \cdot LAI \tag{11}$$

The FAO approach only uses a fixed LAI throughout the growing season. However, LAI plays a dominant role in determining the canopy-atmosphere coupling and ET partitioning (Peng et al, 2019; Wei et al., 2017; Forzieri et al., 2020). In this study, we overcome this limiting assumption by introducing the seasonal cycle of LAI. Kelliher, Leuning, Raupach, & Schulze (1995) found that Gs_{max} estimates are at most three times of the Gst_{max} estimates, therefore we set a maximum limit for $LAI = 4$. For Gst_{max}, the measured values are ranging from 9 mm/s for natural vegetation to 12 mm/s for crops (Kelliher, Leuning, Raupach, & Schulze, 1995), listed in Table 1.

We also used an alternative formula for Gs_{max} from Zhou et al. (2006):

$$Gs_{max} = \frac{LAI_e}{Rst_{min}} \tag{12}$$

where LAI_e is the effective LAI, which is equal to LAI/2 when LAI is greater than 4. Rst_{min} is the minimum stomatal resistance, obtained by the land cover types listed in Table 1 from Zhou et al. (2006).

3.2.3 Albedo

Previous approaches use a fixed grass albedo (0.23) regardless of the underlying land cover type (Allen, Pereira, Raes, & Smith, 1998). In this study, we choose the albedo consistent with the land cover type and explore the option of introducing seasonal cycle of albedo from satellite observations.

3.3 Two source model: separating canopy and soil

The above-mentioned equations in 3.1 and 3.2 treat the surface vegetation as a "big leaf" by considering the canopy resistance and soil resistance together as the bulk surface resistance, and therefore require fewer parameters and less computational costs. One challenge of the big-leaf assumption is to infer bulk surface resistance from canopy resistance when the surface is not fully covered by vegetation (Leuning et al., 2008). Therefore, additionally, we compare the big leaf models with the Shuttle-Wallace (SW) two source model (Shuttleworth and Wallace, 1985; Zhou et al., 2006), incorporating vegetation cover and separating ET into the sum of transpiration and soil evaporation:

$$PET_{SW} = C_c PET_{PMc} + C_s PET_{PMs} \tag{13}$$

where PET_{PMc}, PET_{PMs}, C_c, and C_s are given by Equations 12-18 in Shuttleworth and Wallace (1985). We adopt the same parameterizations detailed in Zhou et al. (2006).

4 Drought quantification

Given the substantial divergence in the PET magnitudes among different models (Peng et al., 2019), a direct comparison of the absolute values among methods is not meaningful. However, the performance in representing drought between PET methods should be comparable. We hypothesize that incorporating the
250   parameters or model structures in Section 3 into the existing methods will increase the accuracy of drought quantification. To test the hypotheses, we use the PM algorithm for big leaf methods, so that we can easily control a specific set of parameters that represents a process option.

We integrate the PET methods into the SPEI drought index across 1-, 3-, 6-, and 12-month time scales over the CONUS. The SPEI is based on the climatological water balance (water supply – atmospheric evaporative
255   demand) cumulated over multiple time scales (e.g., 1, 3, 6, 12 months) following a similar procedure as in the SPI computation (Vicente-Serrano, Beguería, & López-Moreno, 2010). The accumulated water balances are fit using the log-logistic distribution and the probability distribution function is normalized to a standardized variable with mean = 0 and standard deviation = 1, termed as 1-, 3-, 6-, 12-month SPEI, respectively. We calculate the monthly SPEI with the SPEI R package (https://cran.r-
260   project.org/web/packages/SPEI/) using daily meteorological data. We choose the SPEI driven by zero PET as a control scenario to showcase the net effect of introducing existing PET methods into traditional SPI drought index. We choose the SPEI driven by the Open Water (OW) method as the baseline, because the OW approach is the simplest scenario with minimal surface characteristics.

Soil moisture is a direct measure of drought severity. Therefore, we use the correlation between SPEI and
265   soil moisture observations to quantify the skill of PET methods. We aggregated the daily ESA CCI surface soil moisture (SMsurf, m^3 m^{-3}) to monthly averages between 1981-2017 over the CONUS. To match the SPEI on multiple time scales, we calculated the moving average of SMsurf for 1, 3, 6, 12-month periods, respectively. Our analysis focuses on the growing season (April-September), because PET is close to zero during the cold season (not shown). Given the monthly SPEI and SMsurf series during the growing season,
270   Pearson correlation coefficient (R) is calculated for each pair of the SPEI and SMsurf monthly series in each grid cell of the CONUS on the time scale of 1, 3, 6, and 12 months. Then we calculate the change of correlation for each method from the control scenario or the baseline. This change can identify whether a PET method causes an improvement in drought quantification relative to the baseline approach.

275

5 Results

5.1 Overall evaluation of the PET parameterizations

We conducted a pilot analysis to identify the relative importance of different surface characteristics. We selected four existing PET methods and seven testing methods (see Table A1 and Fig. A1 in Appendix A).

280   Note that many methods in these experiments (Table A1) are unrealistic due to the inconsistencies of the surface conditions. Our attention is to include as many combinations as possible for a preliminary analysis. We then compare the CONUS averaged R values between the pairs of PET methods that share the same surface characteristics except for one of the features (Fig. 2).
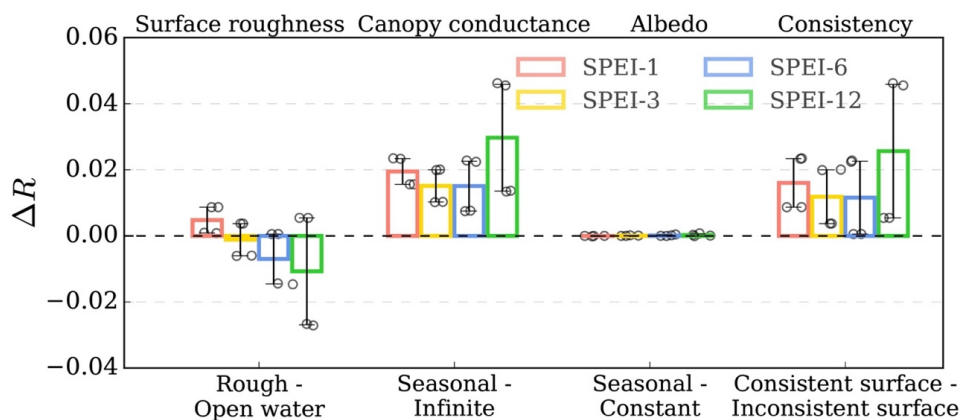
285   **Figure 2. Differences in correlation (ΔR) of pairs of PET methods that share the same surface characteristics except for one of the surface features: surface roughness, canopy conductance, albedo, and overall consistency among the above features.**

Interestingly, activating realistic surface roughness does not necessarily increase, but may even decrease the

290   correlation (ΔR ranging from -0.01 to 0.01 for all time scales). Canopy conductance stands out to be the most important feature for enhancing the skill of drought index (ΔR = 0.015-0.03), meaning that adding the plant phenology driven by LAI can largely improve the seasonal variations of drought index and hence the correlation with SMsurf. We compare ΔR of four pairs with an inconsistent surface (e.g., a combination of open water Ga and seasonal Gc) subtracting from a consistent surface and find that methods with consistent

295   surface features have higher correlations with SMsurf. Surprisingly, seasonal and constant albedo showed no significant difference on the correlations, possibly because of the little variation of albedo during the growing season. The differences in the spatial pattern between constant and seasonal albedo are almost negligible

(Fig. A1). In subsequent sections, we default to using the seasonal albedo in our PET methods to fully represent the surface characteristics.

300   We further compare different parameterizations for Ga and Gc. Here we establish a control scenario where PET is not considered in the SPEI, equivalent to the traditional SPI. The selected PET methods include three traditional methods: OW, RC-short, and RC-tall, four big leaf models and a two source model. We calculated ΔR between each PET method and the control scenario (set PET to zero). Fig. 3 shows ΔR for all grids, forested grids, and nonforested grids using 1-month SPEI. The big leaf methods are grouped by the

305   parameterization of Ga and Gs (Fig. 3 left table).
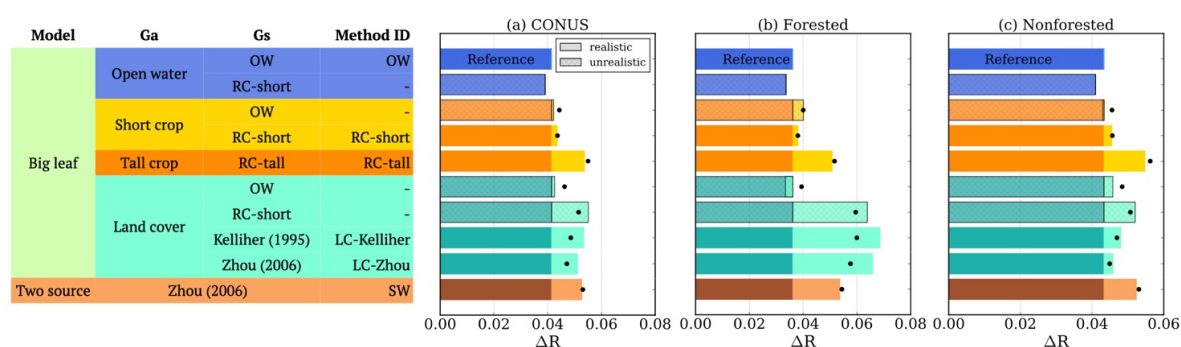
Figure 3. Differences in correlations (ΔR) for selected PET methods versus the control scenario (PET = 0). Correlations were computed between the 1-month SPEI and SMsurf series across: (a) CONUS, (b) forested grids, and (c) nonforested grids. The bars represent the mean ΔR and the black dots
310   **represent the median ΔR. The top blue bars show ΔR in the OW approach versus PET = 0 as a reference. For each bar, the darker shade indicates the reference ΔR and the lighter shade represents any improvement (or decline) relative to the reference. Methods with unrealistic surface conditions are highlighted with a hatch pattern, without any specific Method ID.**

315   Incorporating the benchmark OW method into the SPEI increases R by 0.042, shown by the top horizontal bars. Among the conventional PET methods, the tall reference crop (RC-tall) method stands out. Over the CONUS, it improved ΔR relative to control scenario by 29% more than the OW method (0.054 versus 0.042). The short reference crop (RC-short) method has an identical averaged R with the OW method. Although the RC-tall algorithm (Allen et al., 2005) is less known than the widely used RC-short algorithm (Allen, Pereira,
320   Raes, & Smith, 1998), our results suggest that the SPEI driven by RC-tall correlates better with the SMsurf dynamics.

One encouraging outcome is the performance improvement seen in the two big leaf algorithms incorporating realistic surface conductance. Activating both surface roughness and seasonal Gs produces high correlations of SPEI with SMsurf. These algorithms improve the OW method (ΔR = 0.042) by 24-29% (ΔR is 0.052-0.054). Methods where Ga is determined by land cover (the cyan bars in Fig. 3a) especially improve the correlations with SMsurf (Fig. 3a). It confirms our hypothesis that incorporating realistic vegetation information in atmospheric evaporative demand can enhance drought characterization. Finally, the two source Shuttleworth-Wallace (SW) method outperforms the OW method as expected. However, the SW method produces a similar R as the LC-Kelliher method. This suggests that the simple big leaf model in combination with the land cover details can achieve the same efficacy of the more complicated two source model. While we evaluated several unrealistic methods (see hatch patterns) with inconsistent surface assumptions, most did not outperform the OW method. One exception is the pairing of land cover-specific Ga with the RC-short Ga, which yields a high R.

Over the CONUS, RC-tall, LC-Kelliher, and SW are the top three methods with similar average R. However, when we evaluate the performance in the forested areas (Fig. 3b), LC-Kelliher exhibits the most significant enhancement in ΔR to control scenario, with an increase of 89% over OW's improvement (0.068 relative to 0.036). RC-tall and SW improve ΔR to control scenario by 39% (0.05) and 50% (0.054), respectively. In nonforested areas (Fig. 3c), RC-tall has the best performance, followed by SW. The SW method, designed for sparse vegetation, naturally demonstrates strong performance in these regions. However, it is surprising to see that the simple parametrized RC-tall can outperform SW. Conversely, LC-Kelliher only exhibits a moderate improvement in ΔR. This suggests that, particularly in the sparsely vegetated areas, RC-tall can serve as a strong candidate for PET estimates and drought characterization.

5.2 Spatial patterns analysis

In the subsequent sections, we compare the LC-Kelliher (referred to as LC) method with the three widely used methods: OW, PT, RC-short (simply referred to as RC), and the two source SW method. The time series of these PET methods as well as the SMsurf time series are shown in the Fig. B1. The OW approach serves as the baseline. The highest R is observed for long-term drought (12-month, average R = 0.73) and the lowest is found in medium-term drought (3- and 6-month, average R = 0.48). This suggests that the meteorology-driven SPEI can generally reproduce soil moisture dynamics, especially on an annual time scale.
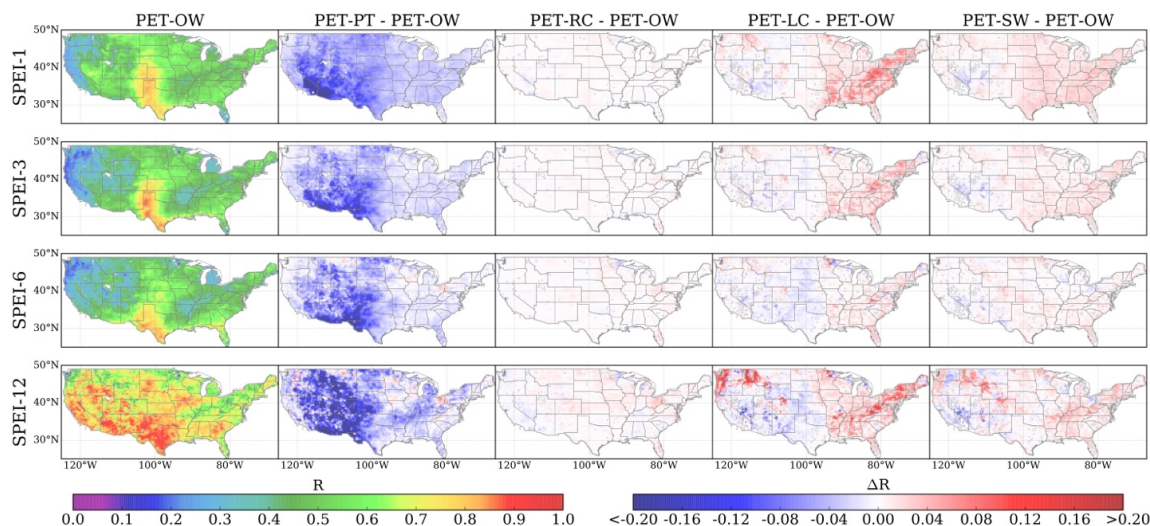
350

Figure 4. The first column displays the correlations between SPEI driven by OW and SMsurf. The four columns on the right show the differences in correlations (ΔR) of PT, RC, LC, and SW relative to OW.

355 Figure 4 displays the spatial distribution of correlations between SPEI driven by OW and SMsurf, along with the differences in correlations of PT, RC-short, LC, and SW compared to OW. PT consistently exhibits lower correlations than OW over most regions, with an average decrease of 0.04, and has especially weak correlations in the southwest U.S. (lower by 0.15). Interestingly, the widely used RC method for SPEI presents little improvement over OW with minimal increases in correlation. LC shows substantial

360 improvements in some areas , with ΔR exceeding 0.16, notably in the eastern and pacific western U.S.. The enhancements of LC are prominent but can be diluted when averaged across CONUS, with ΔR relative to the control scenario 0.012 higher than OW (Fig. 3a). This is especially true when considering LC's less favorable performance in the wouthwest and midwest U.S.. SW also exhibits notable improvements in the eastern and pacific western U.S., with a magnitude of improvement falling between LC and RC. It is encouraging to see

365 that LC outperforms SW in many eastern US grid cells (ΔR = 0.15 versus ΔR = 0.05), given LC's much simpler parameterization. Though it is worth noting that both LC and SW experience performance declines in the Southwest, with LC slightly worse than SW. On the other hand, RC robustly displays improvements in this particular area.
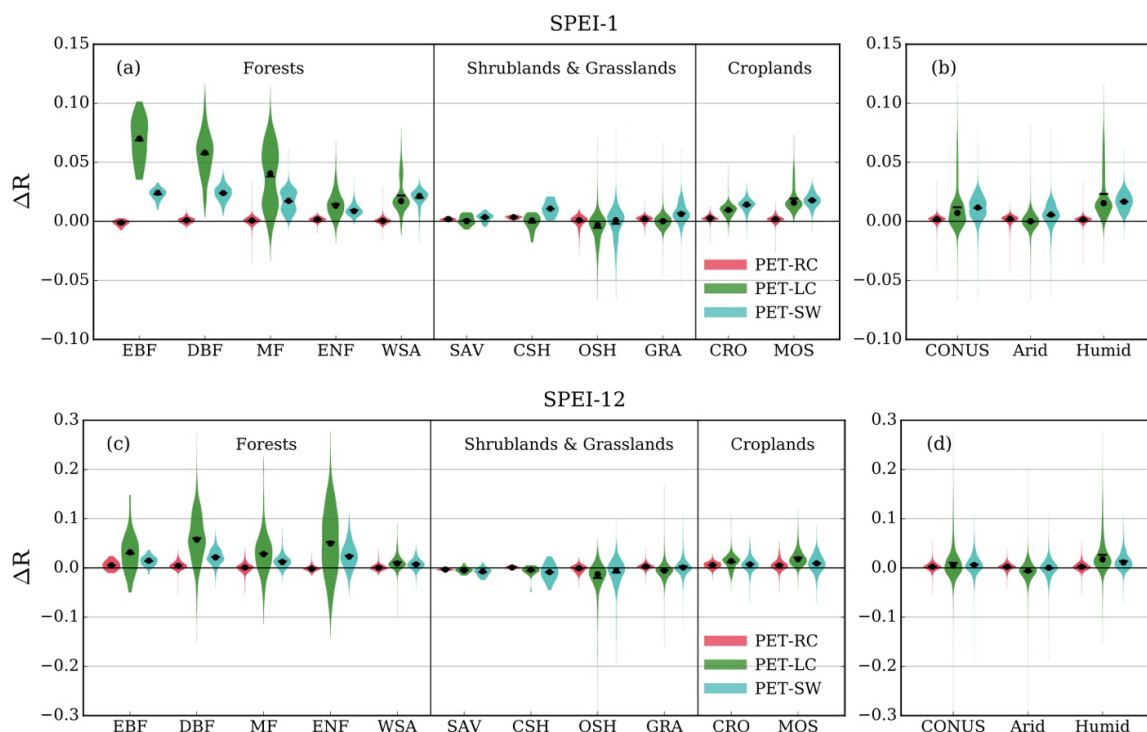
Figure 5. Violin plots of differences in correlations of three PET methods relative to OW, grouped by vegetation types and aridity.

We further delve into the relative performance of these methods summarized by major vegetation types and by aridity (Fig. 5). LC increases *R* significantly in forests, especially in evergreen broadleaf, deciduous broadleaf, and mixed forests, where the largest *ΔR* exceeds 0.1, and the average *ΔR* hovers around or above 0.05 for 1-month scale (Fig. 5a). Notable improvements in evergreen needleleaf forest, woody savanna, and croplands compared to the OW are also observed.

For the time scale of 12-month (Fig. 5c), OW has an already high the average *R* of 0.73 across the CONUS. LC's performance is outstanding in forests, with an average *ΔR* of about 0.05 and the largest *ΔR* even exceeding 0.25. In evergreen needleleaf forests, LC's performance is significantly higher than that of the 1-month time scale. In humid regions, LC's improvements over SW becomes even more apparent compared to the 1-month time scale (Fig. 5d).

In contrast, the average performance of LC in grasslands, shrublands, and savannas (Fig. 5a and c), which are the dominant vegetation types in the western CONUS, are equivalent to OW (except for open shrubland where LC slightly underperforms OW). The magnitude of averaged ΔR of LC is slightly smaller than SW, mainly due to LC's weaker performance in the arid shrublands and grasslands, which cover large portions of the CONUS. Both LC and SW show less advantage or even worse performance than RC and OW in nonforested and arid grid cells (Fig. 5c-d).

6 Discussion

6.1 Interaction between surface features

Figure 2 provides important insights into the SPEI sensitivity to different surface features. Introducing Gs with seasonal vegetation dynamics accounts for most of the total improvement of PET algorithm. This confirms that the FAO approaches are more favored than the OW approach due to its constraints on Gs. This highlights the importance of leaf area index (LAI) as a vegetation feature for drought depiction. LAI is a scaling factor to upscale Gst_{max} to maximum canopy conductance. This is different from the drought index based on the normalized difference vegetation index (NDVI) or LAI, which requires the real-time dynamics of satellite data. This approach only requires the climatology of LAI, which can be easily implemented for drought forecasting where real-time or near-future data are not available.

Using realistic surface roughness does not necessarily improve the overall performance of the SPEI. In fact, the consistency between aerodynamic conductance and surface conductance is more critical for the skill of PET method. Previous study by Peng et al. (2019) explains the linkage between the ratio of actual ET to PET and the ratio of Ga to Gs. When Ga/Gs is large, the ratio of actual ET to PET becomes smaller. Although our study focused on the maximum evapotranspiration given the realistic vegetation condition, such a relationship remains valid. Thus, a large Ga/Gst_{max} ratio should better limit PET with realistic surface constraints. In fact, the LC approach activates surface roughness and increases Ga, while constraining Gst_{max} and reducing Gs. Altogether these factors increase the Ga/Gs ratio and result in significant improvement in capturing the temporal evolution of SMsurf.

6.2 Surface characteristics matter in the forests

Our analysis concludes that incorporating surface features can largely improve the accuracy of drought monitoring in the forests. There are two vegetation groups with significantly improved correlation after incorporating the realistic surface characteristics. Forests over the eastern and pacific western U.S., such as evergreen broadleaf and deciduous broadleaf forests, the LC method exhibits large ΔR compared to OW (up to 0.12 for 1-month and up to 0.25 for 12-month, Fig. 5a, c). While OW has a ΔR at about 0.04 compared to the zero PET control scenario (Fig. 3b), LC has an average ΔR of 0.05 relative to OW in these forests (Fig. 5a). This means the improvement of LC over control scenario is more than doubling of OW. LC also displays a significant increase in R at about 0.025 in woody savanna. The enhancements in the forests or woody savannas are the most predominant since LAI in forests is relatively variable, and surface roughness is also the strongest. Although the southeastern U.S. has a humid subtropic climate, this region also suffered from periodic droughts in 1986–1988, 1998–2002 and 2006–2009 (Seager, Tzanova, & Nakamura, 2009; Pederson

et al., 2012), which is consistent with the increased forest drought severity from 1987-2013 (Peters, Iverson, & Matthews, 2014; Clark et al., 2016). Drought monitoring in these regions is also critical and can benefit from our approach that significantly improve the spatial and temporal accuracy in the forests.

In contrast, the short-grass regions (grasslands, shrublands, and savannas) located in the western U.S. exhibit
425   zero to small improvements for LC. These regions have sparse vegetation cover, and thus LAI plays a less effective role in determining the seasonal dynamics of PET.

6.3 Strategies for PET method selection

We recommend the use of the LC parameterization for drought monitoring in the forests, in which the roughness and surface conductance parameters vary with realistic vegetation conditions. LC is superior than
430   OW or RC-short because of better performance, and compared to SW, it is both better performing and a simpler approach in the forested areas.

For shrublands and grasslands, we recommend the use of RC-tall to replace the more widely used RC-short for drought monitoring. We found that the RC-tall approach has a higher skill than the RC-short approach that is more widely used. The main difference between these two methods is the C_n constant that describes
435   the effect of aerodynamic conductance (Allen et al, 2005). The implementation of tall reference ($C_n = 1600$) seems to work better than the short reference ($C_n = 900$) over the CONUS. It is worth noting, however, that the FAO approaches assume a universal C_n regardless of actual vegetation type. The better skill of RC-tall will not always hold, which may overestimate PET in semi-arid non-vegetated regions.

For sparse vegetation, since the responses of the components of evapotranspiration to the environmental
440   drivers are different (Katul, Oren, Manzoni, Higgins, & Parlange, 2012; Or & Lehmann, 2019), the partitioning between canopy and soil can also play a role in determining AED. The SW model significantly improves the SPEI skill driven by the OW approach. It outperforms LC in the shrublands and grasslands. Despite its complexity, it is a good choice for drought monitoring in these vegetation types.

For croplands, we recommend choosing between RC-tall versus RC-short based on the actual crop canopy
445   height. The more realistic approach is to use RC-tall for higher crops. Lastly, the PT method has the poorest correlation with soil moisture and is unlikely to capture drought dynamics.

6.4 Bridging gaps in drought prediction

Motivated by the question of whether incorporating surface characteristics can improve drought prediction, we overcome several limitations of previous drought quantification methods. Firstly, our study presents a
450   different approach whereby we focus on the maximum possible evapotranspiration for a given vegetation

condition. This concept allows a physically meaningful definition of evaporative demand for the non-uniform land surfaces.

Secondly, the ultimate goal of PET calculation is to simulate ET and to quantify drought. Despite the simplicity of calculating PET using the existing Penman-type methods, the biggest challenge for assessing these methods is validation. Since the real evaporative demand rate is unattainable from observations, it is challenging to validate which PET method is superior directly. Even using ET observations for PET validation can be problematic because biased PET estimates and wrong surface biophysical parameters can still produce accurate ET estimates for locations with ET measurements (Peng et al., 2019). Our study evaluates the PET methods by comparing drought index with independently observed soil moisture (Vicente-Serrano et al., 2012). This approach helps diagnose the most appropriate PET approach for drought quantification directly while avoiding the complexity and divergence caused by various PET definitions.

Finally, our approach bridges the gap between the two methodologies for quantifying soil-moisture drought, which is of most relevance to agriculture (Seneviratne, 2012). Since soil moisture observations are limited by inadequate measurement networks, drought indices such as the SPEI are often used to quantify drought. In hydrology, a drought index is a simple water balance model driven by surface meteorology without the use of any surface characteristics. Its shortcomings are the neglect of seasonally varying vegetation cover and the incapability to capture the vegetation control on transpiration. An alternative is to use land surface models to estimate large-scale soil moisture (Sheffield, & Wood, 2007). This approach often builds in vegetation dynamics and can provide temporally consistent soil moisture simulations, but it also requires substantial efforts to prepare meteorological forcings at high temporal resolution, set up the domain, spin up, and calibrate. Our approach is a compromise between the above two types of models, which is more realistic and process-based than the commonly used drought index while being easy-to-implement and less data-intensive than a land surface model.

475

7 Conclusions

To understand whether incorporating surface characteristics can improve drought prediction, we revise current PET methods in a newly developed drought index (SPEI), using the concept of maximum ET for any given vegetation condition. We use a simple look-up table approach combining in situ measurements and large-scale data fusion products for the key surface and aerodynamic parameters,. This study also presents a novel application of independent soil moisture observations to diagnose the most appropriate PET approach for drought quantification. Our approach is proved to be more effective than widely used big leaf methods and two source model in accurately predicting soil moisture spatiotemporal dynamics in the forests and humid regions. LAI has a particularly important influence on the skill of the SPEI. This new yet simple approach strikes a balance between a meteorology-driven water balance model and a complex land surface model for drought prediction. It could improve the accuracy of the drought reconstruction in forests and displays great potential to improve real-time drought forecast.

Appendix A. Initial examination of PET methods and parameterizations

490   We conduct a preliminary analysis to identify the importance of surface characteristics. Each of the above processes are regarded as different options: (i) using active surface roughness or open water surface, (ii) seasonally varying or fixed surface conductance, and (iii) seasonally varying or fixed surface albedo.

Table A1 provides the PET methods and the parameters in the preliminary analysis. The first set of methods (a-d) are the existing physically-based PET approaches: the open-water Penman equation (OW), the FAO
495   reference crop evapotranspiration for tall crop and short crop, and the Priestley-Taylor equation (PT).

Table A1. Summary of the PET methods with their ID, name and abbreviation code, and details about surface characteristics.

ID	Method (Code)	Ga		Gs_{max}			Albedo (α)	
		Open Water	Rough surface	Infinite	Constant	Seasonal	Constant	Seasonal
a	Open Water (OW)	X		X			X	
b	FAO Tall reference crop (RC-tall)		X		X		X	
c	FAO Short reference crop (RC-short)		X		X		X	
d	Priestley-Taylor (PT)						X	
e	Open Water Ga/ Infinite Gc/ Seasonal α (GAow_GSinf_ALBs)	X		X				X
f	Open Water Ga/ Seasonal Gc/ Constant α (GAow_GSs_ALBc)	X				X	X	
g	Open Water Ga/ Seasonal Gc/ Seasonal α (GAow_GSs_ALBs)	X				X		X
h	Rough Ga/ Seasonal Gs/ Seasonal α (GAr_GSs_ALBs)		X			X		X
i	Rough Ga/ Infinite Gc/ Constant α (GAr_GSinf_ALBc)		X	X			X	
j	Rough Ga/ Infinite Gc/ Seasonal α (GAr_GSinf_ALBs)		X	X				X
k	Rough Ga/ Seasonal Gc/ Constant α (GAr_GSs_ALBc)		X			X	X	

We examine seven algorithms (e-k) to isolate the effects of surface characteristics on PET. First, in methods

500 (e), (f), (g), the aerodynamic conductance module is not active as we set Ga to the open water Ga_{ow}, indicating a smooth surface with low roughness (Equation 6). In methods (h), (i), (j), (k), we activate aerodynamic conductance using realistic surface roughness (Equation 9). Second, in methods (e), (i), (j), the surface conductance parameter is unconstrained as we set Gst_{max} to infinity. In methods (f), (g), (h), (k), we activate surface conductance using seasonal LAI dynamics and Gst_{max} from Kelliher et al. (1995). Lastly,

505 in methods (f), (i), (k), the albedo parameter is not active as we set α to a constant (grass: 0.23, water: 0.08). In methods (e), (g), (h), (j), we activate albedo parameter using seasonal albedo dynamics.
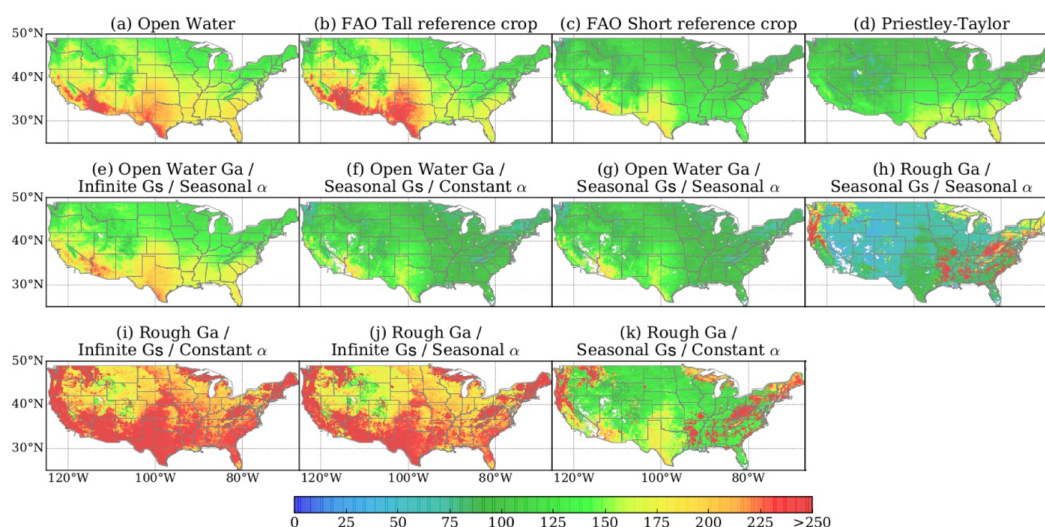
Figure A1. Growing season averages of AED derived from four PET methods and seven testing algorithms over the CONUS. Details and ID for each method are listed in Table A1.

510

Figure A1 displays the spatial patterns of growing season averages of these methods. For the classical Penman/Penman-Monteith methods (Fig. A1a-c), the highest mean growing season AED values are found in southern California, Arizona, and Texas, while the PT method (Fig. A1d) predicts the largest AED values in Texas and Florida. The spatial patterns of PET based on the rough surface (Fig. A1h-l, Rough Ga) are very

515 different from those methods that assume a universal reference height (Fig. A1b-c, reference crop) or open water surface (Fig. A1a, e-g). Specifically, the regions which exhibit large PET estimates (> 250 mm/mon, Fig. A1h-k) are forests, such as ENF in the Pacific Northwest, DBF in the Northeast, and MF in the southeastern U.S.. Interestingly, although the methods using constant albedo (α=0.08) have generally larger

520 AED values than those using seasonal albedo, the differences in the spatial pattern between the two are almost negligible (Fig. A1a vs. A1e, Fig. A1i vs. A1j, Fig. A1k vs. A1h).

The combination of the rough aerodynamic and unconstrained surface conductance, represented by (i) GAr_GSinf_ALBc and (j) GAr_GSinf_ALBs, produces extremely high monthly PET values with means at 330 to 340 mm/mon. The remaining methods also predict a wide range of mean monthly totals. On average, the big-leaf method GAr_GSs_ALBs (Fig. A1h) provides the smallest PET estimates.

525 Assessing the change between pairs of the above methods can identify whether adding/removing a surface feature eventually causes an improvement in drought quantification (Fig. 2). The first feature surface roughness is determined by the way Ga is estimated. We compare the parameter set between rough and the open water surface by calculating the differences (Rough - Open Water) for the following pairs of experiments: (i) GAr_GSinf_ALBc - (a) OW, (j) GAr_GSinf_ALBs - (e) GAow_GSinf_ALBs, and (k)

530 GAr_GSs_ALBc - (f) GAow_GSs_ALBc. In terms of the canopy conductance, we calculate the differences between seasonal and infinite Gs_{max} (Seasonal - Infinite) for the following pairs of experiments: (f) GAow_GSs_ALBc - (a) OW, (g) GAow_GSs_ALBs - (e) GAow_GSinf_ALBs, and (k) GAr_GSs_ALBc - (i) GAr_GSinf_ALBc.

535

Appendix B. Temporal evolution of PET methods, SPEIs, and SMsurf
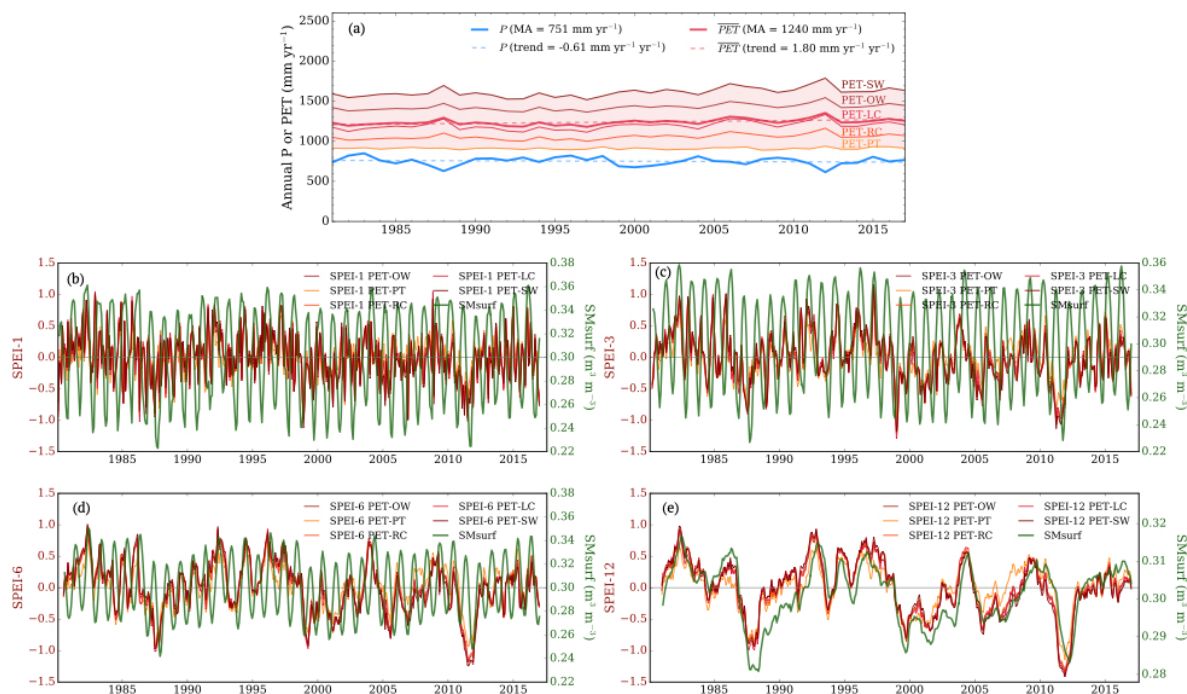
Figure B1. a) The annual precipitation and PET (mm yr⁻¹) from five key methods between 1981-2017.
b)-e) SPEI series driven by the five PET methods, aligning with the SMsurf time series for four time
scales: 1, 3, 6, 12-month.

540

Code and data availability

The model codes are available online at https://github.com/pitcheverlasting (will become a public repo after acceptance).

545   The data generated in our study are published in this public repository:
https://doi.org/10.6084/m9.figshare.12132696.v1. (active after acceptance).

The primary data and tools can be downloaded from the PRISM Climate Group at Oregon State University
(http://www.prism.oregonstate.edu), the ESA CCI soil moisture project team (https://www.esa-
soilmoisture-cci.org/node/145), the GIMMS LAI3g product team

550   (https://drive.google.com/open?id=0BwL88nwumpqYaFJmR2poS0d1ZDQ), the Global Land Surface
Satellite project (http://www.glass.umd.edu/Download.html), the SPEI R package released by Santiago
Beguería and Sergio M. Vicente-Serrano at CSIC in Spain (https://cran.r-project.org/web/packages/SPEI/),
the Global Land Cover Climatology project
(https://archive.usgs.gov/archive/sites/landcover.usgs.gov/global_climatology.html), and the CDO software

555   (https://code.zmaw.de/projects/cdo).

Author contributions

LP and JS conceived the idea, LP designed and implemented the PET experiments and analyzed the data.
LP wrote the paper with contributions from ZW, ME, and EFW.

Competing interests

560   The authors declare that they have no conflict of interest.

Acknowledgements

This research has been supported by NASA under grant NNX14AB36A. We thank Dan Li at Boston
University for the helpful discussions. We thank Philip Lu for proofreading.

565   **References**

Acreman, M. C., Harding, R. J., Lloyd, C. R., & McNeil, D. D. (2003). Evaporation characteristics of
wetlands: experience from a wetgrassland and a reedbed using eddy correlation measurements. *Hydrology
and Earth System Sciences*, *7*(1), 11–21. http://doi.org/10.5194/hess-7-11-2003

Allen, R. G., Pereira, L. S., Raes, D., & Smith, M. (1998). Crop evapotranspiration-Guidelines for
570   computing crop water requirements-FAO Irrigation and drainage paper 56. *FAO*, *300*(9), D05109.

Allen, R. G., Walter, I. A., Elliott, R., Howell, T. A., Itenfisu, D., & Jensen, M. (2005). *The ASCE
standardized reference evapotranspiration equation* (p. 4). Reston, VA 20191: American Society of Civil
Engineers.

Andreadis, K. M., Clark, E. A., Wood, A. W., Hamlet, A. F., & Lettenmaier, D. P. (2005). Twentieth-
575   Century Drought in the Conterminous United States. *Journal of Hydrometeorology*, *6*(6), 985–1001.
https://doi.org/10.1175/jhm450.1

Andreadis, K. M., & Lettenmaier, D. P. (2006). Trends in 20th century drought over the continental United
States. *Geophysical Research Letters*, *33*(10). https://doi.org/10.1029/2006gl025711

Barbeta, A., Ogaya, R., & Peñuelas, J. (2013). Dampening effects of long-term experimental drought on
580   growth and mortality rates of a Holm oak forest. *Global Change Biology*, *19*(10), 3133–3144.
https://doi.org/10.1111/gcb.12269

Beguería, S., Vicente-Serrano, S. M., Reig, F., & Latorre, B. (2013). Standardized precipitation
evapotranspiration index (SPEI) revisited: parameter fitting evapotranspiration models, tools, datasets and
drought monitoring. *International Journal of Climatology*, *34*(10), 3001–3023.
585   https://doi.org/10.1002/joc.3887

Broxton, P. D., Zeng, X., Sulla-Menashe, D., & Troch, P. A. (2014). A Global Land Cover Climatology
Using MODIS Data. *Journal of Applied Meteorology and Climatology*, *53*(6), 1593–1605.
https://doi.org/10.1175/jamc-d-13-0270.1

Brutsaert, W. (1982). The Surface Roughness Parameterization. In A. J. Davenport, B. B. Hicks, G. R.
590   Hilst, R. E. Munn, & J. D. Smith (Eds.), *Evaporation into the Atmosphere* (pp. 113–127). Dordrecht:
Springer Netherlands. https://doi.org/10.1007/978-94-017-1497-6_5

Brutsaert, W., & Stricker, H. (1979). An advection-aridity approach to estimate actual regional
evapotranspiration. *Water Resources Research*, *15*(2), 443–450. https://doi.org/10.1029/wr015i002p00443

Campbell, G. S., & Norman, J. M. (1998). Wind. In *An introduction to environmental biophysics* (pp. 68-
595   70). New York, NY: Springer.

Clark, J. S., Iverson, L., Woodall, C. W., Allen, C. D., Bell, D. M., Bragg, D. C., … Zimmermann, N. E.
(2016). The impacts of increasing drought on forest dynamics structure, and biodiversity in the United
States. *Global Change Biology*, *22*(7), 2329–2352. https://doi.org/10.1111/gcb.13160

Dai, A., Trenberth, K. E., & Qian, T. (2004). A Global Dataset of Palmer Drought Severity Index for
600   18702002: Relationship with Soil Moisture and Effects of Surface Warming. *Journal of
Hydrometeorology*, *5*(6), 1117–1130. https://doi.org/10.1175/jhm-386.1

Daly, C., Halbleib, M., Smith, J. I., Gibson, W. P., Doggett, M. K., Taylor, G. H., … Pasteris, P. P. (2008).
Physiographically sensitive mapping of climatological temperature and precipitation across the
conterminous United States. *International Journal of Climatology*, *28*(15), 2031–2064.
605   https://doi.org/10.1002/joc.1688

Daly, C., Neilson, R. P., & Phillips, D. L. (1994). A Statistical-Topographic Model for Mapping
Climatological Precipitation over Mountainous Terrain. *Journal of Applied Meteorology*, *33*(2), 140–158.
https://doi.org/10.1175/1520-0450(1994)033<0140:astmfm>2.0.co;2

Dewes, C. F., Rangwala, I., Barsugli, J. J., Hobbins, M. T., & Kumar, S. (2017). Drought risk assessment
610   under climate change is sensitive to methodological choices for the estimation of evaporative demand. *Plos
One*, *12*(3), e0174045. http://doi.org/10.1371/journal.pone.0174045

Dong, C., MacDonald, G. M., Willis, K., Gillespie, T. W., Okin, G. S., & Williams, A. P. (2019).
Vegetation Responses to 20122016 Drought in Northern and Southern California. *Geophysical Research
Letters*, *46*(7), 3810–3821. https://doi.org/10.1029/2019gl082137

615   Dorigo, W., Wagner, W., Albergel, C., Albrecht, F., Balsamo, G., Brocca, L., … Lecomte, P. (2017). ESA
CCI Soil Moisture for improved Earth system understanding: State-of-the art and future directions. *Remote
Sensing of Environment*, *203*, 185–215. https://doi.org/10.1016/j.rse.2017.07.001

Ek, M. B., Mitchell, K. E., Lin, Y., Rogers, E., Grunmann, P., Koren, V., et al. (2003). Implementation of
Noah land surface model advances in the National Centers for Environmental Prediction operational
620   mesoscale Eta model. *Journal of Geophysical Research*, *108*(D22), 2002JD003296.
http://doi.org/10.1029/2002JD003296

Fang, L., Zhan, X., Hain, C. R., Yin, J., & Liu, J. (2018). Impact of GVF Derivation Methods on Noah Land Surface Model Simulations and WRF Model Forecasts. *Journal of Hydrometeorology*, *19*(12), 1917–1933. https://doi.org/10.1175/jhm-d-18-0075.1

625   Feng, S., Trnka, M., Hayes, M., & Zhang, Y. (2017). Why Do Different Drought Indices Show Distinct Future Drought Risk Outcomes in the U.S. Great Plains?. *Journal of Climate*, *30*(1), 265–278. https://doi.org/10.1175/jcli-d-15-0590.1

Forzieri, G., G Miralles, D., Ciais, P., Alkama, R., Ryu, Y., Duveiller, G., et al. (2020). Increased control of vegetation on global terrestrial energy fluxes. *Nature Climate Change*, *4*(2), 1–7.

630   http://doi.org/10.1038/s41558-020-0717-0

Gruber, A., Dorigo, W. A., Crow, W., & Wagner, W. (2017). Triple collocation-based merging of satellite soil moisture retrievals. *IEEE Transactions on Geoscience and Remote Sensing*, *55*(12), 6780-6792. https://doi.org/10.1109/TGRS.2017.2734070.

Gruber, A., Scanlon, T., van der Schalie, R., Wagner, W., & Dorigo, W. (2019). Evolution of the ESA CCI

635   Soil Moisture climate data records and their underlying merging methodology. *Earth System Science Data*, *11*, 717-739. https://doi.org/10.5194/essd-11-717-2019

Heim, R. R. (2002). A Review of Twentieth-Century Drought Indices Used in the United States. *Bulletin of the American Meteorological Society*, *83*(8), 1149–1166. https://doi.org/10.1175/1520-0477-83.8.1149

Hobbins, M. T., Wood, A., Streubel, D., & Werner, K. (2012). What Drives the Variability of Evaporative

640   Demand across the Conterminous United States? *Journal of Hydrometeorology*, *13*(4), 1195–1214. http://doi.org/10.1175/JHM-D-11-0101.1

Hoerling, M., Eischeid, J., Kumar, A., Leung, R., Mariotti, A., Mo, K., … Seager, R. (2014). Causes and Predictability of the 2012 Great Plains Drought. *Bulletin of the American Meteorological Society*, *95*(2), 269–282. https://doi.org/10.1175/bams-d-13-00055.1

645   Katul, G. G., Oren, R., Manzoni, S., Higgins, C., & Parlange, M. B. (2012). Evapotranspiration: A process driving mass transport and energy exchange in the soil-plant-atmosphere-climate system. *Reviews of Geophysics*, *50*(3). https://doi.org/10.1029/2011rg000366

Kelliher, F. M., Leuning, R., Raupach, M. R., & Schulze, E.-D. (1995). Maximum conductances for evaporation from global vegetation types. *Agricultural and Forest Meteorology*, *73*(1-2), 1–16.

650   https://doi.org/10.1016/0168-1923(94)02178-m

Kogan, F. N. (1995). Droughts of the Late 1980s in the United States as Derived from NOAA Polar-Orbiting Satellite Data. *Bulletin of the American Meteorological Society*, *76*(5), 655–668. https://doi.org/10.1175/1520-0477(1995)076<0655:dotlit>2.0.co;2

Kustas, W. P., Choudhury, B. J., Moran, M. S., Reginato, R. J., Jackson, R. D., Gay, L. W., & Weaver, H. L. (1989). Determination of sensible heat flux over sparse canopy using thermal infrared data. *Agricultural and Forest Meteorology*, *44*(3-4), 197–216. https://doi.org/10.1016/0168-1923(89)90017-8

Leuning, R., Zhang, Y. Q., Rajaud, A., Cleugh, H., & Tu, K. (2008). A simple surface conductance model to estimate regional evaporation using MODIS leaf area index and the Penman-Monteith equation. *Water Resources Research*, *44*(10), 1872. http://doi.org/10.1029/2007WR006562

Lhomme, J.-P., Troufleau, D., Monteny, B., Chehbouni, A., & Bauduin, S. (1997). Sensible heat flux and radiometric surface temperature over sparse Sahelian vegetation II. A model for the kB-1 parameter. *Journal of Hydrology*, *188-189*, 839–854. https://doi.org/10.1016/s0022-1694(96)03173-3

Liang, X., Lettenmaier, D. P., Wood, E. F., & Burges, S. J. (1994). A simple hydrologically based model of land surface water and energy fluxes for general circulation models. *Journal of Geophysical Research: Atmospheres (1984–2012)*, *99*(D7), 14415–14428. http://doi.org/10.1029/94JD00483

Liu, Q., Wang, L., Qu, Y., Liu, N., Liu, S., Tang, H., & Liang, S. (2013). Preliminary evaluation of the long-term GLASS albedo product. *International Journal of Digital Earth*, *6*(sup1), 69–95. https://doi.org/10.1080/17538947.2013.804601

Liu, Y. Y., Dorigo, W. A., Parinussa, R. M., de Jeu, R. A. M., Wagner, W., McCabe, M. F., … van Dijk, A. I. J. M. (2012). Trend-preserving blending of passive and active microwave soil moisture retrievals. *Remote Sensing of Environment*, *123*, 280–297. https://doi.org/10.1016/j.rse.2012.03.014

Loon, A. F. V. (2015). Hydrological drought explained. *Wiley Interdisciplinary Reviews: Water*, *2*(4), 359–392. https://doi.org/10.1002/wat2.1085

Lorenz, R., Davin, E. L., Lawrence, D. M., Stö Ckli, R., & Seneviratne, S. I. (2013). How important is vegetation phenology for European climate and heat waves? *Journal of Climate*, *26*(24), 10077–10100. http://doi.org/10.1175/JCLI-D-13-00040.1

Martens, B., Miralles, D. G., Lievens, H., van der Schalie, R., de Jeu, R. A. M., Fernández-Prieto, D., … Verhoest, N. E. C. (2017). GLEAM v3: satellite-based land evaporation and root-zone soil moisture. *Geoscientific Model Development*, *10*(5), 1903–1925. https://doi.org/10.5194/gmd-10-1903-2017

680 McDowell, N. G., Allen, C. D., Teixeira, K. A., Brando, P., Brienen, R., Chambers, J., et al. (2018). Drivers and mechanisms of tree mortality in moist tropical forests. *New Phytologist*, *219*(3), 851–869. http://doi.org/10.1111/nph.15027

McKee, T. B., Doesken, N. J., Kleist, J., & others. (1993). The relationship of drought frequency and duration to time scales. In *Proceedings of the 8th Conference on Applied Climatology* (Vol. 17, pp. 179–
685 183). Boston, MA: American Meteorological Society.

Monteith, J. L. (1965). Evaporation and environment. *Symposia of the Society for Experimental Biology*, *19*, 205–234.

Monteith, J., & Unsworth, M. (2013). Micrometeorology. In *Principles of environmental physics: plants, animals, and the atmosphere* (pp. 301-310). Academic Press.

690 Moran, M. S., Rahman, A. F., Washburne, J. C., Goodrich, D. C., Weltz, M. A., & Kustas, W. P. (1996). Combining the Penman-Monteith equation with measurements of surface temperature and reflectance to estimate evaporation rates of semiarid grassland. *Agricultural and Forest Meteorology*, *80*(2-4), 87–109. http://doi.org/10.1016/0168-1923(95)02292-9

Nadeau, D. F., Brutsaert, W., Parlange, M. B., Bou-Zeid, E., Barrenetxea, G., Couach, O., … Vetterli, M.
695 (2009). Estimation of urban sensible heat flux using a dense wireless network of observations. *Environmental Fluid Mechanics*, *9*(6), 635–653. https://doi.org/10.1007/s10652-009-9150-7

Norman, J. M., Kustas, W. P., & Humes, K. S. (1995). Source approach for estimating soil and vegetation energy fluxes in observations of directional radiometric surface temperature. *Agricultural and Forest Meteorology*, *77*(3-4), 263–293. https://doi.org/10.1016/0168-1923(95)02265-y

700 Or, D., & Lehmann, P. (2019). Surface Evaporative Capacitance: How Soil Type and Rainfall Characteristics Affect Global-Scale Surface Evaporation. *Water Resources Research*, *55*(1), 519–539. https://doi.org/10.1029/2018wr024050

Palmer, W. C. (1965). *Meteorological drought* (Vol. Research paper No. 45, p. 58). Washington, DC: U.S. Weather Bureau.

705 Paulo, A. A., Rosa, R. D., & Pereira, L. S. (2012). Climate trends and behaviour of drought indices based on precipitation and evapotranspiration in Portugal. *Natural Hazards and Earth System Sciences*, *12*(5), 1481–1491. https://doi.org/10.5194/nhess-12-1481-2012

Pederson, N., Bell, A. R., Knight, T. A., Leland, C., Malcomb, N., Anchukaitis, K. J., … Riddle, J. (2012). A long-term perspective on a modern drought in the American Southeast. *Environmental Research Letters*, *7*(1), 014034. https://doi.org/10.1088/1748-9326/7/1/014034

Peng, L., Li, D., & Sheffield, J. (2018). Drivers of Variability in Atmospheric Evaporative Demand: Multiscale Spectral Analysis Based on Observations and Physically Based Modeling. *Water Resources Research*, *54*(5), 3510–3529. http://doi.org/10.1029/2017WR022104

Peng, L., Zeng, Z., Wei, Z., Chen, A., Wood, E. F., & Sheffield, J. (2019). Determinants of the ratio of actual to potential evapotranspiration. *Global change biology*, *25*(4), 1326-1343. https://doi.org/10.1111/gcb.14577

Penman, H. L. (1948). Natural evaporation from open water, bare soil and grass. *Proceedings of the Royal Society of London Series A*, *193*, 120–145.

Peters, M. P., Iverson, L. R., & Matthews, S. N. (2014). *Spatio-temporal trends of drought by forest type in the conterminous United States, 1960-2013*. U.S. Department of Agriculture Forest Service, Northern Research Station. https://doi.org/10.2737/nrs-rmap-7

Potop, V. (2011). Evolution of drought severity and its impact on corn in the Republic of Moldova. *Theoretical and Applied Climatology*, *105*(3-4), 469–483. https://doi.org/10.1007/s00704-011-0403-2

Potop, V., Možný, M., & Soukup, J. (2012). Drought evolution at various time scales in the lowland regions and their impact on vegetable crops in the Czech Republic. *Agricultural and Forest Meteorology*, *156*, 121–133. https://doi.org/10.1016/j.agrformet.2012.01.002

Priestley, C. H. B., & Taylor, R. J. (1972). On the assessment of surface heat flux and evaporation using large-scale parameters. *Monthly Weather Review*, *100*(2), 81–92.

Qu, Y., Liu, Q., Liang, S., Wang, L., Liu, N., & Liu, S. (2014). Direct-Estimation Algorithm for Mapping Daily Land-Surface Broadband Albedo From MODIS Data. *IEEE Transactions on Geoscience and Remote Sensing*, *52*(2), 907–919. https://doi.org/10.1109/tgrs.2013.2245670

Rigden, A., Li, D., & Salvucci, G. (2018). Dependence of thermal roughness length on friction velocity across land cover types: A synthesis analysis using AmeriFlux data. *Agricultural and Forest Meteorology*, *249*, 512–519. https://doi.org/10.1016/j.agrformet.2017.06.003

Ross, T., & Lott, N. (2003). A climatology of 1980-2003 extreme weather and climate events. *National Climatic Data Center Technical Report*, *1*, 14.

Seager, R., Tzanova, A., & Nakamura, J. (2009). Drought in the Southeastern United States: Causes Variability over the Last Millennium, and the Potential for Future Hydroclimate Change. *Journal of Climate*, *22*(19), 5021–5045. https://doi.org/10.1175/2009jcli2683.1

740 Sellers, P. J., Randall, D. A., Collatz, G. J., Berry, J. A., Field, C. B., Dazlich, D. A., et al. (1996). A revised land surface parameterization (SiB2) for atmospheric GCMs .1. Model formulation, *9*(4), 676–705.

Seneviratne, S. I., Corti, T., Davin, E. L., Hirschi, M., Jaeger, E. B., Lehner, I., et al. (2010). Investigating soil moisture–climate interactions in a changing climate: A review. *Earth-Science Reviews*, *99*(3-4), 125–161. http://doi.org/10.1016/j.earscirev.2010.02.004

745 Seneviratne, S. I. (2012). Historical drought trends revisited. *Nature*, *491*(7424), 338–339. http://doi.org/10.1038/491338a

Sheffield, J., & Wood, E. F. (2007). Characteristics of global and regional drought, 1950–2000: Analysis of soil moisture data from off-line simulation of the terrestrial hydrologic cycle. *Journal of Geophysical Research: Atmospheres (1984–2012)*, *112*(D17), D17115. http://doi.org/10.1029/2006JD008288

750 Sheffield, J., Wood, E. F., & Roderick, M. L. (2012). Little change in global drought over the past 60 years. *Nature*, *491*(7424), 435–438. https://doi.org/10.1038/nature11575

Shuttleworth, W. J. (1993). Chapter 4 Evaporation. In D. R. Maidment (Ed.), *Handbook of hydrology* (Vol. 9780070). Sydney: McGraw-Hill.

Simard, M., Pinto, N., Fisher, J. B., & Baccini, A. (2011). Mapping forest canopy height globally with
755 spaceborne lidar. *Journal of Geophysical Research: Biogeosciences*, *116*(G4). https://doi.org/10.1029/2011JG001708

Stewart, J. B., Kustas, W. P., Humes, K. S., Nichols, W. D., Moran, M. S., & de Bruin, H. A. R. (1994). Sensible Heat Flux-Radiometric Surface Temperature Relationship for Eight Semiarid Areas. *Journal of Applied Meteorology*, *33*(9), 1110–1117. https://doi.org/10.1175/1520-
760 0450(1994)033<1110:shfrst>2.0.co;2

Trenberth, K. E., Dai, A., van der Schrier, G., Jones, P. D., Barichivich, J., Briffa, K. R., & Sheffield, J. (2013). Global warming and changes in drought. *Nature Climate Change*, *4*(1), 17–22. https://doi.org/10.1038/nclimate2067

Troufleau, D., Lhomme, J. P., Monteny, B., & Vidal, A. (1997). Sensible heat flux and radiometric surface temperature over sparse Sahelian vegetation. I. An experimental analysis of the kB-1 parameter. *Journal of Hydrology*, *188-189*, 815–838. https://doi.org/10.1016/s0022-1694(96)03172-1

Verhoef, A., Bruin, H. A. R. D., & Hurk, B. J. J. M. V. D. (1997). Some Practical Notes on the Parameter kB-1 for Sparse Vegetation. *Journal of Applied Meteorology*, *36*(5), 560–572. https://doi.org/10.1175/1520-0450(1997)036<0560:spnotp>2.0.co;2

Verma, S. B. (1989). Aerodynamic resistances to transfers of heat, mass and momentum. In: Black, T. A., Spittlehouse, D. L., Novak, M. D., Price, D. T. (Eds.), *Estimation of Areal Evapotranspiration* (pp. 13-20). IAHS Press.

Vicente-Serrano, S. M., Beguería, S., Lorenzo-Lacruz, J., Camarero, J. J., López-Moreno, J. I., Azorin-Molina, C., … Sanchez-Lorenzo, A. (2012). Performance of Drought Indices for Ecological Agricultural, and Hydrological Applications. *Earth Interactions*, *16*(10), 1–27. https://doi.org/10.1175/2012ei000434.1

Vicente-Serrano, S. M., Beguería, S., & López-Moreno, J. I. (2010). A Multiscalar Drought Index Sensitive to Global Warming: The Standardized Precipitation Evapotranspiration Index. *Journal of Climate*, *23*(7), 1696–1718. https://doi.org/10.1175/2009jcli2909.1

Vicente-Serrano, S. M., Gouveia, C., Camarero, J. J., Begueria, S., Trigo, R., Lopez-Moreno, J. I., … Sanchez-Lorenzo, A. (2013). Response of vegetation to drought time-scales across global land biomes. *Proceedings of the National Academy of Sciences*, *110*(1), 52–57. https://doi.org/10.1073/pnas.1207068110

Vicente-Serrano, S. M., der Schrier, G. V., Beguería, S., Azorin-Molina, C., & Lopez-Moreno, J.-I. (2015). Contribution of precipitation and reference evapotranspiration to drought indices under different climates. *Journal of Hydrology*, *526*, 42–54. https://doi.org/10.1016/j.jhydrol.2014.11.025

Wei, Z., Yoshimura, K., Wang, L., G Miralles, D., Jasechko, S., & Lee, X. (2017). Revisiting the contribution of transpiration to global terrestrial evapotranspiration. *Geophysical Research Letters*, *44*(6), 2792–2801. http://doi.org/10.1002/2016GL072235

Wilhite, D. A. (2000), Drought as a natural hazard: Concepts and definitions, In *Drought: A Global Assessment* (pp. 3-18). London: Routledge.

Wilhite, D. A., Sivakumar, M. V. K., & Pulwarty, R. (2014). Managing drought risk in a changing climate: The role of national drought policy. *Weather and Climate Extremes*, *3*, 4–13. https://doi.org/10.1016/j.wace.2014.01.002

Williams, A. P., Allen, C. D., Macalady, A. K., Griffin, D., Woodhouse, C. A., Meko, D. M., et al. (2012). Temperature as a potent driver of regional forest drought stress and tree mortality. *Nature Climate Change*,

795   *3*(3), 292–297. http://doi.org/10.1038/nclimate1693

Xia, Y., Mitchell, K., Ek, M., Sheffield, J., Cosgrove, B., Wood, E., … Mocko, D. (2012). Continental-scale water and energy flux analysis and validation for the North American Land Data Assimilation System project phase 2 (NLDAS-2): 1. Intercomparison and application of model products. *Journal of Geophysical Research: Atmospheres*, *117*(D3), n/a–n/a. https://doi.org/10.1029/2011jd016048

800   Yan, H., Wang, S. Q., Billesbach, D., Oechel, W., Zhang, J. H., Meyers, T., … Scott, R. (2012). Global estimation of evapotranspiration using a leaf area index-based surface energy and water balance model. *Remote Sensing of Environment*, *124*, 581–595. https://doi.org/10.1016/j.rse.2012.06.004

Yang, K., Koike, T., Ishikawa, H., Kim, J., Li, X., Liu, H., … Wang, J. (2008). Turbulent Flux Transfer over Bare-Soil Surfaces: Characteristics and Parameterization. *Journal of Applied Meteorology and*

805   *Climatology*, *47*(1), 276–290. https://doi.org/10.1175/2007jamc1547.1

Yang, R., & Friedl, M. A. (2003). Determination of Roughness Lengths for Heat and Momentum Over Boreal Forests. *Boundary-Layer Meteorology*, *107*(3), 581–603. https://doi.org/10.1023/a:1022880530523

Yang, Y., Roderick, M. L., Zhang, S., McVicar, T. R., & Donohue, R. J. (2019). Hydrologic implications of vegetation response to elevated CO2 in climate projections. *Nature Climate Change*, *9*(1), 44–48.

810   https://doi.org/10.1038/s41558-018-0361-0

Zhang, L., Jiao, W., Zhang, H., Huang, C., & Tong, Q. (2017). Studying drought phenomena in the Continental United States in 2011 and 2012 using various drought indices. *Remote Sensing of Environment*, *190*, 96–106. https://doi.org/10.1016/j.rse.2016.12.010

Zhao, H., Gao, G., An, W., Zou, X., Li, H., & Hou, M. (2017). Timescale differences between SC-PDSI

815   and SPEI for drought monitoring in China. *Physics and Chemistry of the Earth Parts A/B/C*, *102*, 48–58. https://doi.org/10.1016/j.pce.2015.10.022

Zhou, M. C., Ishidaira, H., Hapuarachchi, H. P., Magome, J., Kiem, A. S., & Takeuchi, K. (2006). Estimating potential evapotranspiration using Shuttleworth–Wallace model and NOAA-AVHRR NDVI data to feed a distributed hydrological model over the Mekong River basin. *Journal of Hydrology*, 327(1-

820   2), 151-173. https://doi.org/10.1016/j.jhydrol.2005.11.013

Zhu, Z., Bi, J., Pan, Y., Ganguly, S., Anav, A., Xu, L., … Myneni, R. (2013). Global Data Sets of Vegetation Leaf Area Index (LAI)3g and Fraction of Photosynthetically Active Radiation (FPAR)3g

Derived from Global Inventory Modeling and Mapping Studies (GIMMS) Normalized Difference
Vegetation Index (NDVI3g) for the Period 1981 to 2011. *Remote Sensing*, *5*(2), 927–948.

825 https://doi.org/10.3390/rs5020927

Zilitinkevich, S. S., Grachev, A. A., & Fairall, C. W. (2001). Scaling Reasoning and Field Data on the Sea
Surface Roughness Lengths for Scalars. *Journal of the Atmospheric Sciences*, *58*(3), 320–325.
https://doi.org/10.1175/1520-0469(2001)058<0320:nacraf>2.0.co;2